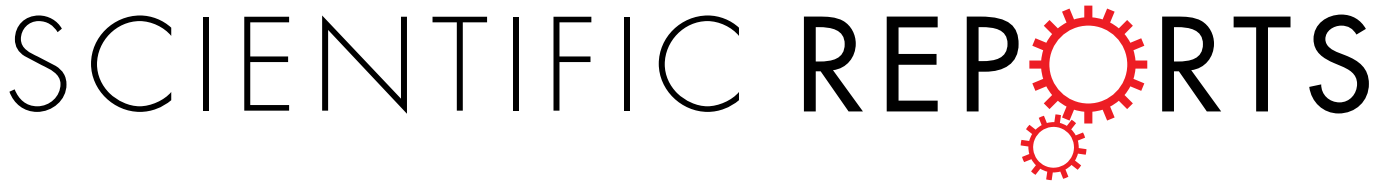

OPEN

Ultra-high electrochemical catalytic activity of MXenes

Hui Pan

Received: 29 April 2016
Accepted: 10 August 2016
Published: 08 September 2016

Cheap and abundant electrocatalysts for hydrogen evolution reactions (HER) have been widely pursued for their practical application in hydrogen-energy technologies. In this work, I present systematical study of the hydrogen evolution reactions on MXenes (Mo_2X and W_2X, X = C and N) based on density-functional-theory calculations. I find that their HER performances strongly depend on the composition, hydrogen adsorption configurations, and surface functionalization. I show that W_2C monolayer has the best HER activity with near-zero overpotential at high hydrogen density among all of considered pure MXenes, and hydrogenation can efficiently enhance its catalytic performance in a wide range of hydrogen density further, while oxidization makes its activity reduced significantly. I further show that near-zero overpotential for HER on Mo_2X monolayers can be achieved by oxygen functionalization. My calculations predict that surface treatment, such as hydrogenation and oxidization, is critical to enhance the catalytic performance of MXenes. I expect that MXenes with HER activity comparable to Pt in a wide range of hydrogen density can be realized by tuning composition and functionalizing, and promotes their applications into hydrogen-energy technologies.

As an important energy carrier, hydrogen is clean, abundant, and renewable, and has been extensively investigated for its practical applications in green-energy technologies. Series of hydrogen-related technologies have been developed for their practical applications, such as hydrogen production and utilization in fuel cell[1–6]. Hydrogen evolution reaction (HER) is involved in the electrochemical reactions of both these technologies and determines the efficiencies of hydrogen production and utilization. The electrocatalyst used in these technologies plays a key role on the efficient HER reactions. Currently, noble metals, such as platinum and palladium, are most common electrocatalysts in electrolysis of water and fuel cell because of their high catalytic performance in HER[7–12]. However, their ultra-high cost and very-low abundance are detrimental to the commercialization of these technologies on large scale. Extensive efforts have been carried out to reduce the amounts of noble metals by alloying with cheap metals and tuning the composition of the catalysts[7–12]. Alternatively, novel electrocatalysts with low cost and rich abundance have been widely investigated to replace noble-metal catalysts[13–35]. Especially, two-dimensional (2D) monolayers as electrocatalysts, such as 2D transition-metal dichalcogenides monolayers (TMDs), have been attracting increasing interests because of their unique physical and chemical properties[20–35]. Experimental and theoretical studies showed that the electrocatalytic activity strongly depended on their structure, conductivity, edge states, defects, tensile strain, etc[20–35]. For example, the electrocatalytic activities of semiconducting TMDs in electrolysis of water were contributed to their metallic edges[25,29]. Further studies showed that the surfaces of metallic TMDs showed better HER performance than semiconducting counterparts[26,28,31,33]. However, most TMDs only showed electrocatalytic activity at low hydrogen coverage on surfaces or at edges because their conductivities were reduced or metallic TMDs changed to semiconducting ones as hydrogen coverage increases, which dramatically limits their practical applications[33].

Recently, a new family of 2D monolayers, MXenes, were discovered[36–52]. The MXenes are transitional-metal carbides/nitrides monolayers and have a general formula, $M_{i+1}X_i$, where "M" is transition metal element, "X" is C or N, and i is a positive integer[36]. These monolayer with various thicknesses can be simply obtained by exfoliating layered ternary transition metal carbides/nitrides ($M_{i+1}AX_i$), where "A" is main group element (group IIIA and IVA)[36]. Most recently, Xu *et al.* reported the growth of large-scale high quality, superconducting 2D Mo_2C monolayer by chemical vapour deposition[52]. Theoretical and experimental studies showed that most of MXenes are metallic. As learnt from the noble metals and MX_2 monolayers/nanoribbons, it is well-known that the high conductivity of electrocatalyst is the prerequisite to the excellent HER activity. It is, therefore, that MXenes may find applications as electrocatalysts in hydrogen-related green energy technologies. To date, the study on the HER performances of MXenes has not been available. In this work, the electrocatalytic performance of MXenes for

Institute of Applied Physics and Materials Engineering, Faculty of Science and Technology, University of Macau, Macao SAR. Correspondence and requests for materials should be addressed to H.P. (email: huipan@umac.mo)

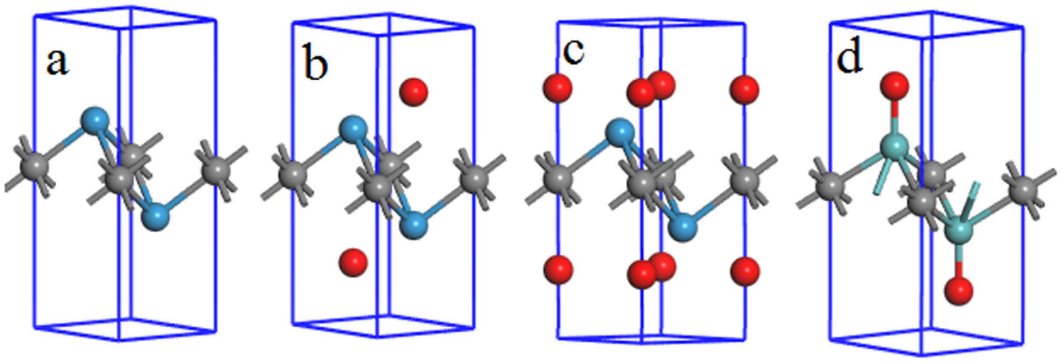

Figure 1. The representative structures of (**a**) pristine M_2X and M_2X with both sides covered by atoms (red) at different positions: (**b**) HC, (**c**) TX, and (**d**) TM. By removing red atoms from one side of the monolayer, one-side coverage is realized.

their applications as catalysts in HER is investigated based on the calculations of density-functional theory (DFT). It is predicted that the HER performances of MXenes strongly depend on their composition, surface treatment, hydrogen coverage, and hydrogen adsorption sites. It is found that pure and hydrogenated W_2C monolayers are excellent in HER in a wide range of hydrogen density, while oxidization results in the significant reduction of its HER ability. It is shown that oxidized Mo_2X monolayer is much better than pure and hydrogenated counterparts in HER. It is suggested that surface treatment is crucial to the applications of MXenes as electrocatalysts in HER.

Results

Geometric structure. In the calculations, I focus on molybdenum- and tungsten-based MXenes, M_2X (M = Mo and W; X = C and N). M_2X monolayer is a three-atom-thick layer in a sequence of M1-X-M2 (Fig. 1a), and X-atom layer is enclaved in M-atom layers, leading to M_6N octahedron. The unit cells of these MXenes are fully relaxed to obtain their lattice constants and study their electronic properties. It is noticed that the lattice constants of M_2C MXenes are larger than those of M_2N, and the lattice constants of Mo_2X are larger than those of W_2X (Table 1). The calculated total density of states (TDOSs) show that M_2X monolayers are metallic (Supporting Data, S1), indicating their potential applications as electrocatalysts in HER.

Hydrogen adsorption. To investigate their HER abilities, the lattice parameters of hydrogen-covered MXenes need to be calculated. Generally, there are three possible sites for hydrogen atoms to be adsorbed on the monolayers, including top of hexagonal center (HC) (Fig. 1b), top of X atom (TX) (Fig. 1c), and top of M atom (TM) (Fig. 1d). To give a full understanding on the effect of hydrogen coverage on their HER abilities, two cases are considered, including one side and both sides of MXenes covered by hydrogen atoms. The unit cells of MXenes with various hydrogen coverages at different adsorption sites are fully relaxed to find the stable adsorption position and obtain lattice parameters. For simplicity, these MXenes with various hydrogen coverages at different adsorption sites are named as M_2XH_m-Ad, where m = 1 (H-coverage on one side of monolayer) and m = 2 (H-coverage on both sides of monolayer), and "Ad" is the adsorption site and can be HC, TX, and TM. The relaxed geometries show that the adsorption of hydrogen atoms on HC and TX of MXene unit cell has negligible effect on the lattice constants, while that on TM results in the lattice extension by 1~8% (Table 1). At the same time, the thicknesses of the monolayers are increased by ~5% when hydrogen atoms adsorb on HC and TX, but reduced by 10~20% for hydrogen adsorption on TM. As an indication of stable adsorption, the adsorption energy (E_{ad}) is calculated as below:

$$E_{ad} = (E(M_2XH_m) - E(M_2X) - \frac{m}{2}E(H_2))/m \quad (1)$$

where $E(M_2XH_m)$ and $E(M_2X)$ are the total energies of MXene unit cell with and without H atoms (m), and $E(H_2)$ is the energy of hydrogen molecule (H_2). m is 1 for H-coverage on one side of monolayer or 2 for H-coverage on its both sides. Our calculations shows that the adsorption energies are negative at all of three possible sites (Fig. 2), indicating that all of the sites may be possible to host hydrogen atoms. It is found that HC is the most stable site to host hydrogen atom, followed by TX, and then by TM because the adsorption energy (negative) increases as the adsorption site changing from HC → TX → TM (Fig. 2). It is also found that the adsorption energy difference between two sites on W_2C monolayer is the smallest among all of the considered MXenes. The variation of adsorption energy may affect the HER ability of MXenes.

HER activity of pure MXenes. Basically, an advanced catalyst for the enhanced electrochemical hydrogen evolution reaction should reduce the HER reaction overpotential and consequently increase the HER efficiency, which can be quantified by the reaction Gibbs free energy of hydrogen adsorption (ΔG_H)[9–11,53]. To investigate the hydrogen-coverage (H-coverage) dependent HER activity of pure MXene, a supercell with $2 \times 2 \times 1$ unit cells is constructed based on the unit of MXene with one surface fully covered by hydrogen atoms at different adsorption sites (M_2XH-Ad). Partial H-coverage is realized by removing H atom one by one from the H-covered surface of

	a (Å)	c (Å)	X-M (Å)	H-M (Å)
Mo_2C	2.978	2.368	2.088	
Mo_2CH-HC	2.928	2.533	2.139/2.082	1.981
Mo_2CH-TX	2.971	2.405	2.120/2.059	2.059
Mo_2CH-TM	3.085	2.199	2.086/2.100	1.712
Mo_2CH_2-HC	2.960	2.498	2.112	2..002
Mo_2CH_2-TX	2.951	2.458	2.101	2.058
Mo_2CH_2-TM	3.063	2.300	2.109	1.716
Mo_2N	2.798	2.799	2.137	
Mo_2NH-HC	2.791	2.854	2.170/2.135	1.982
Mo_2NH-TX	2.804	2.831	2.168/2.133	1.993
Mo_2NH-TM	2.831	2.759	2.160/2.117	1.696
Mo_2NH_2-HC	2.791	2.876	2.159	1.978
Mo_2NH_2-TX	2.797	2.916	2.176	1.992
Mo_2NH_2-TM	3.103	2.168	2.095	1.705
W_2C	2.874	2.657	2.125	
W_2CH-HC	2.885	2.668	2.149/2.119	1.994
W_2CH-TX	2.917	2.571	2.133/2.105	2.039
W_2CH-TM	3.027	2.337	2.102/2.103	1.714
W_2CH_2-HC	2.909	2.654	2.141	2.003
W_2CH_2-TX	2.941	2.526	2.116	2.068
W_2CH_2-TM	3.048	2.368	2.119	1.717
W_2N	2.787	2.897	2.165	
W_2NH-HC	2.779	2.949	2.192/2.166	1.995
W_2NH-TX	2.790	2.945	2.192/2.173	1.992
W_2NH-TM	2.815	2.882	2.201/2.144	1.696
W_2NH_2-HC	2.778	2.982	2.189	2.000
W_2NH_2-TX	2.790	3.000	2.200	1.992
W_2NH_2-TM	2.846	2.856	2.177	1.701

Table 1. Lattice parameters of pure and hydrogenated MXene monolayers: M_2X (M = Mo and W; X = C and N). a is lattice constant, c is the thickness of the monolayer in vertical direction, X-M is the bond length, and H-M is the hydrogen-metal distance.

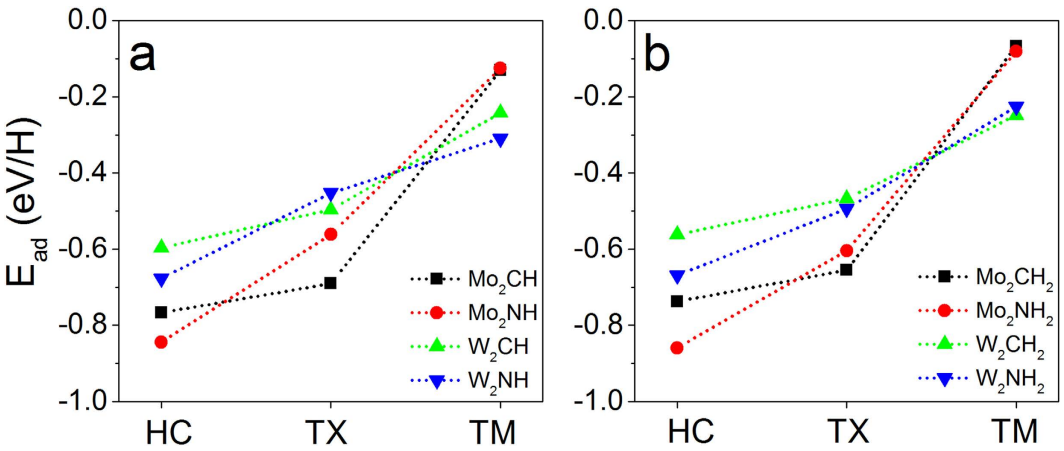

Figure 2. Calculated H-adsorption energy at different sites on M_2X monolayers: (**a**) one-side H-coverage and (**b**) two-side H-coverage.

M_2XH-Ad and the calculation on H-coverage-dependent HER performance is carried out accordingly. The H-coverage is defined as $\frac{n}{4}$ (n = 0~4). The H-coverage dependent ΔG_H can be calculated as below[10,11,31,53]:

$$\Delta G_H = \Delta E_H + \Delta E_{ZPE} - T\Delta S_H \quad (2)$$

where ΔE_H is the hydrogen chemisorption energy. It can be differential chemisorption energy as calculated from:

$$\Delta E_H = E(M_2X + nH) - E(M_2X + (n-1)H) - \frac{1}{2}E(H_2) \quad (3)$$

or, be average chemisorption energy as calculated from:

$$\Delta E_H = (E(M_2X + nH) - E(M_2X) - \frac{n}{2}E(H_2))/n \quad (4)$$

where n (= 0~4) is the number of H atoms adsorbed on one side of a M_2X monolayer. The H-coverage-dependent ΔG_H can be obtained by changing n. $E(M_2X+nH)$ and $E(M_2X)$ in Eqs (3) and (4) are the energies of monolayer supercell with variable hydrogen atoms (n) and pure M_2X supercell, respectively. ΔS_H is the difference in entropy and T is room temperature. ΔE_{ZPE} is the difference in zero point energy between the adsorbed and the gas phase. $\Delta E_{ZPE} - T\Delta S_H$ is about 0.24 eV. Therefore, Eq. (2) can be simplified to $\Delta G_H = \Delta E_H + 0.24$. According to the two methods (Eqs (3) and (4)) for the calculation of hydrogen chemisorption energy, the Gibbs free energies are defined as differential ΔG_H (d-ΔG_H) and average ΔG_H (a-ΔG_H), which can be used to express the HER activities in the individual and collective processes, respectively. The individual process describes that hydrogen is produced one by one, while the collective process shows that all of hydrogen atoms on the surface are simultaneously converted to molecules. In principle, an electrocatalyst with optimal HER performance should have a ΔG_H near 0 eV.

The calculated ΔG_H shows that the HER activities of M_2X monolayers strongly depend on the H-coverage and adsorption sites (Fig. 3). For M_2X monolayers with H adsorbed on HC (M_2X-HC), the calculated Gibbs free energies are negative and increase with the increment of H-coverage in both individual and collective processes (Fig. 3a,b). The W_2X monolayers are better than Mo_2X in the HER activity because of their relatively lower overpotentials (absolute values of ΔG_H). Especially, the d-ΔG_H of W_2C-HC is about −0.15 eV at full H-coverage (n = 4) (Fig. 3a), indicating good HER performance at high H-density in individual process. The calculated average Gibbs free energies (a-ΔG_H) for M_2X-HC are less than −0.3 eV (Fig. 3b). The collective processes are more difficult to take place than individual processes because the total energy in the collective process needs to multiply the number hydrogen atoms removed from the surface, which are far away from 0 eV (Fig. 3b).

If the hydrogen atoms adsorb on TX sites of M_2X monolayers (M_2X-TX), it is found that the HER activities are improved because of relatively lower overpotentials (Fig. 3c,d) at the same H-coverage compared to M_2X-HC (Fig. 3a,b). In particular, the differential Gibbs free energies of W_2C-TX and W_2N-TX monolayers at full H-coverage (n = 4) are −0.05 and 0.09 eV (Fig. 3c), respectively, which are much near zero than those with H atoms adsorbed on HC sites (−0.14 eV for W_2C and −0.21 eV for W_2N, Fig. 3a). Similarly, the collective processes are difficult because their overpotentials are larger than those in individual processes (Fig. 3c,d).

Different from H atoms adsorbed on HC and TX, all of considered MXenes with H atoms adsorbed on TM show good HER activities at certain H-coverage because of near zero overpotentials in both individual and collective processes (Fig. 3e,f). For example, Mo_2N monolayer (Mo_2N-TM) shows the best HER performance at low H-coverage in both individual and collective processes due to near-zero d-ΔG_H (−0.008 eV for n = 1 and −0.001 eV for n = 2) (Fig. 3e) and a-ΔG_H (−0.008 eV for n = 1 and −0.004 eV for n = 2) (Fig. 3f). W_2C monolayer (W_2C-TM) still shows the best HER activity with d-ΔG_H = −0.02 eV at high H-coverage (n = 4) in individual process (Fig. 3e). Mo_2C-TM is excellent for HER reactions at low hydrogen density in individual process (d-ΔG_H = −0.1 for n = 1 and −0.06 for n = 2) (Fig. 3e) and at high hydrogen density in collective process (a-ΔG_H = −0.04 eV for n = 3 and 0.03 eV for n = 4) (Fig. 3f). Clearly, the weak chemical-adsorption leads to the enhancement of HER activity (Fig. 3).

HER activity of MXenes with one side hydrogenated. It had been reported that MXene can be easily functionalized by H, OH, and F, which affect their performance in energy storage[40,41,43]. To study the effect of hydrogenation on HER activity, a supercell with 2 × 2 × 1 unit cells is constructed based on the unit of MXene with both surfaces fully covered by hydrogen atoms at different adsorption sites (M_2XH_2-Ad). By removing H atom one by one from one of its surfaces, the effect of hydrogenation on the H-coverage dependent HER activity can be evaluated. To calculate the Gibbs free energies, it only needs to replace M_2X in Eqs (3) and (4) by M_2XH. Therefore, $E(M_2XH+nH)$ is the energy of monolayer with one side covered with variable hydrogen atoms (n) and another side fully covered by hydrogen atoms (M_2XH-Ad-nH), and $E(M_2XH)$ is the energy of M_2X monolayer with one side fully covered by hydrogen atoms (M_2XH-Ad). The calculated overpotentials show that hydrogenation can efficiently improve the HER activities of M_2X monolayers (Fig. 4). For M_2X monolayer with hydrogenation at HC sites on one of its surfaces (M_2XH-HC), the HER activities are improved because of the reduced overpotentials in individual processes (Fig. 4a). In particular, the d-ΔG_H of W_2C monolayer is about 0.05 eV at full H-coverage (n = 4), which just satisfies the basic requirement for an efficient electrocatalyst with $\Delta G_H = 0$ eV. Although the average Gibbs free energies (a-$\Delta G_H < 0$) for M_2XH-HC in collective processes are increased (Fig. 4b), they are still less than −0.2 eV, indicating that the collective processes are difficult to take place.

Interestingly, the hydrogenation on one side of W_2C monolayer with H atoms at TX sites (W_2CH-TX) can efficiently improve its catalytic performance at high H-density (Fig. 4c). The calculated differential Gibbs free energies of W_2CH-TX are close to zero at high H-coverage (−0.04 and 0.02 eV for n = 3 and 4), indicating excellent HER performance. The calculated average Gibbs free energies (negative) (Fig. 4d) are less than differential ones (Fig. 4c), indicating that collective process is also difficult to happen.

Hydrogenation dramatically affect the HER performances of M_2XH-TM monolayers in both individual and collective processes (Fig. 4e,f). It is found that all of M_2XH-TM monolayers show excellent HER activities at certain H-coverage in both processes. The calculated d-ΔG_H and a-ΔG_H on Mo_2CH-TM are −0.04 eV at n = 1. The Gibbs free energies in individual processes are −0.03 eV for Mo_2NH-TM and −0.02 eV for W_2NH-TM at n = 3, respectively. Although the HER activity of W_2CH-TM is reduced at n = 4 (d-ΔG_H = 0.12 eV), it is strongly

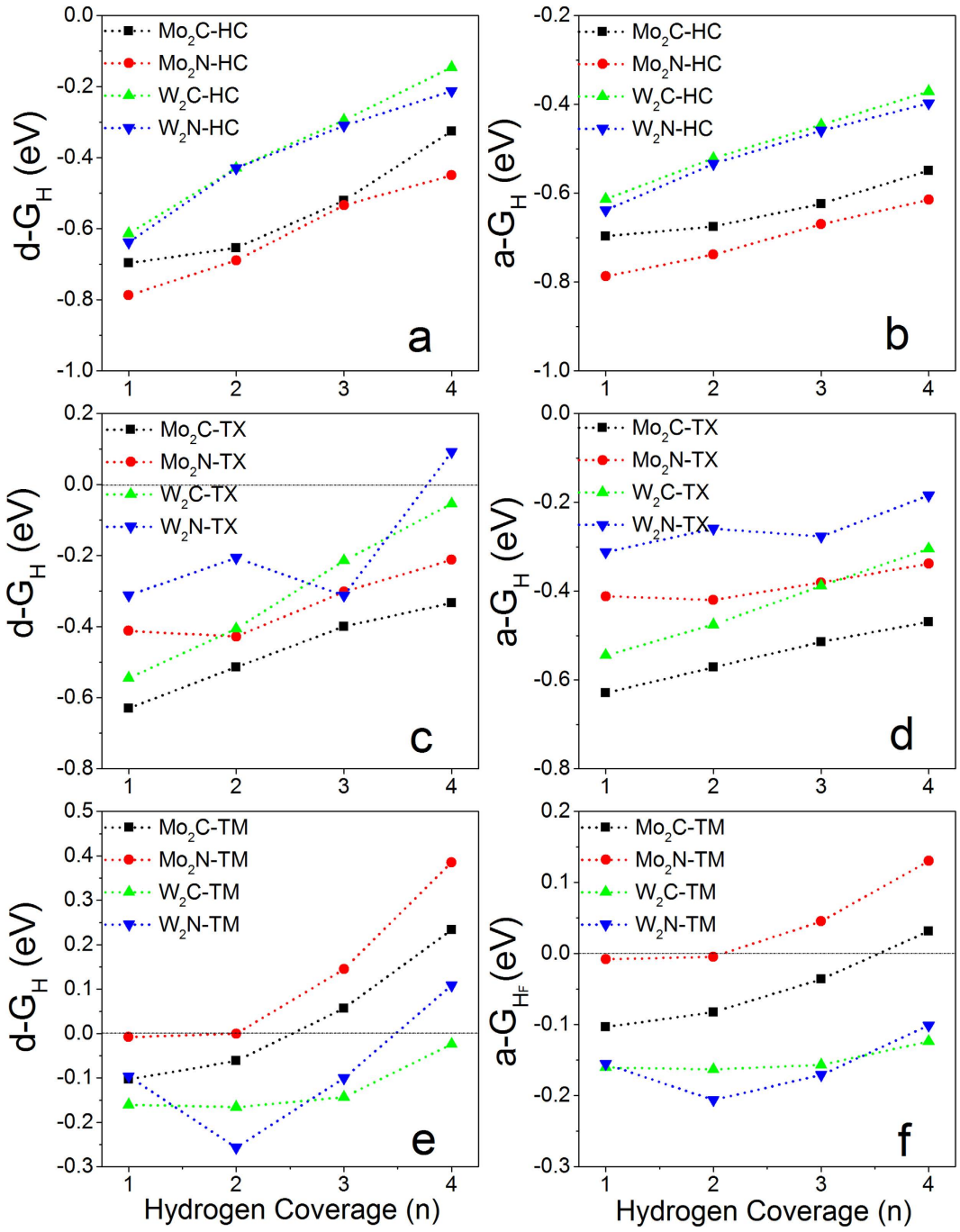

Figure 3. Calculated differential Gibbs free energy as a function of H-coverage on pure M_2X monolayers (M_2X-Ad) with H atoms adsorbed on: (**a**) HC, (**c**) TX, and (**e**) TM; Calculated average Gibbs free energy as a function of H-coverage on pure M_2X monolayers with H atoms adsorbed on: (**b**) HC, (**d**) TX, and (**f**) TM.

improved at n = 3 (d-$\Delta G_H = -0.01$ eV) in individual process (Fig. 4e). Importantly, the calculated a-ΔG_H for Mo_2NH-TM and W_2CH-TM are about −0.04 eV at full H-coverage (n = 4) and that for W_2NH-TM is about −0.02 eV at n = 3 (Fig. 4f), indicating the collective processes can take place. Compared to pure MXenes (Fig. 3), it is found that hydrogenation can efficiently enhance their HER performance, especially in the collective processes.

HER activity of oxidized MXenes. Beside hydrogenation, the MXenes are also easily oxidized. In the section, I focus on the effect of oxygen-functionalization on their HER activities. The MXenes with two sides oxidized are named as M_2XO_2 (M = Mo and W, and X = C and N). There are three possible sites for oxygen to cover the surfaces M_2X monolayers (Fig. 1b–d). The unit cells of M_2XO_2-Ad monolayers (Ad = HC, TX, and TM) are fully relaxed to obtain the stable adsorption site. It is found that M_2XO_2-HC and M_2XO_2-TX are more stable

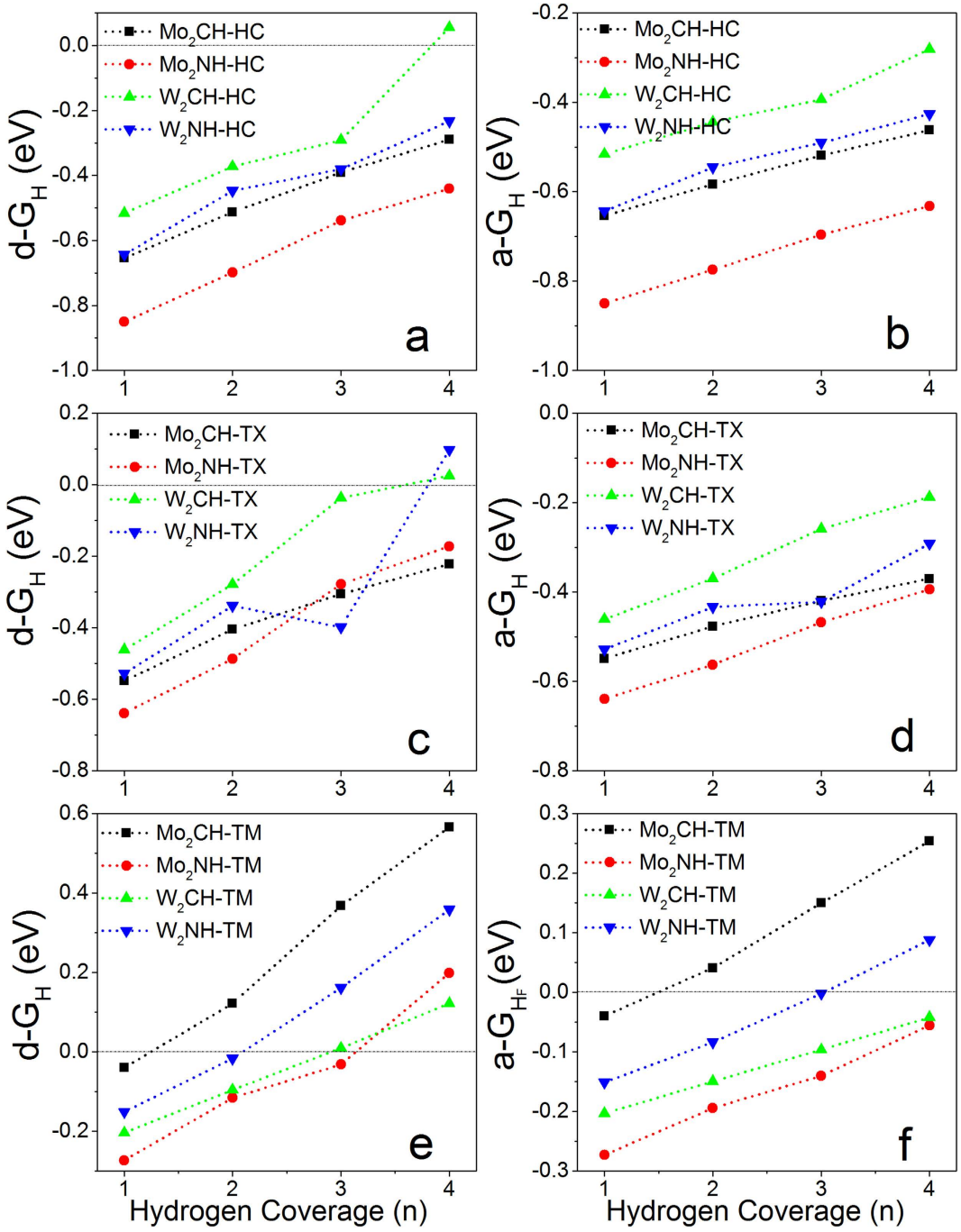

Figure 4. Calculated differential Gibbs free energy as a function of H-coverage on one-side hydrogenated M_2X monolayers (M_2XH-Ad) with H atoms adsorbed on: (**a**) HC, (**c**) TX, and (**e**) TM; Calculated average Gibbs free energy as a function of H-coverage on one-side hydrogenated M_2X monolayers with H atoms adsorbed on: (**b**) HC, (**d**) TX, and (**f**) TM.

than M_2XO_2-TM because their energies are low by ~3–4 eV/unit, and M_2XO_2-TX is more stable than M_2XO_2-HC by an energy of 0.7–1.2 eV/unit (Fig. 5). To investigate their applications in HER reactions, both M_2XO_2-HC and M_2XO_2-TX are studied because the adsorption of hydrogen may lead to phase transition. The unit cells of M_2XO_2 monolayers with H atoms adsorbed on the tops of oxygen atoms (M_2XO_2-mH-Ad, m = 1 and 2, Ad = HC and TX) are optimized (insets in Fig. 5). Our calculations show that the energy differences between M_2XO_2-1H-TX and M_2XO_2-1H-HC was reduced to 0.05~0.26 eV when one side is fully covered by hydrogen atoms, except Mo_2NO_2-1H (Fig. 5). Mo_2NO_2-1H-HC is more stable than Mo_2NO_2-1H-TX by an energy of 0.6 eV (Fig. 5), indicating phase transition from Mo_2NO_2-TX to Mo_2NO_2-HC. When both sides of M_2XO_2 monolayers are covered by hydrogen atoms (M_2XO_2-2H), phase transitions take place in all systems because M_2XO_2-2H-HC is more stable than M_2XO_2-2H-TX by an energy of 0.02~0.82 eV (Fig. 5). The calculated lattice constants of M_2XO_2-Ad

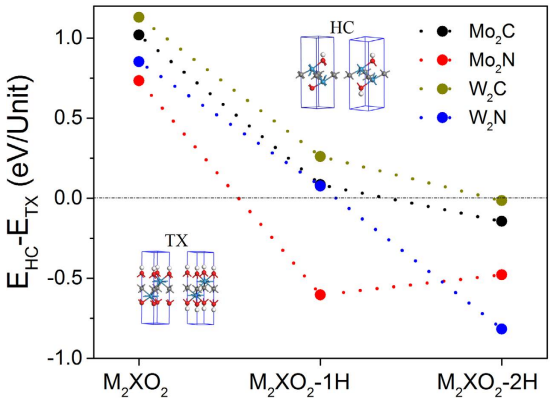

Figure 5. Calculate energy differences of M_2X monolayers with oxidization at different sites and H-adsorption. The insets show the oxidized M_2X monolayers with H atoms at HC and TX sites, respectively.

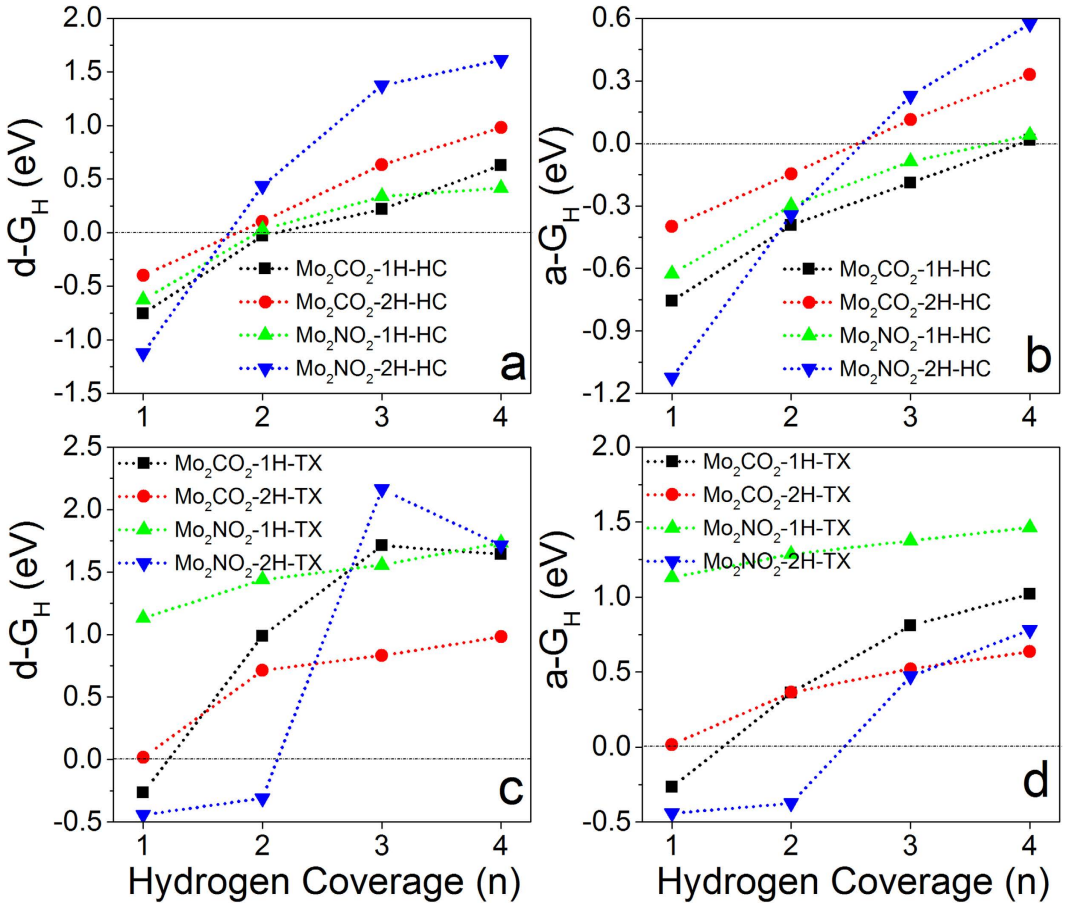

Figure 6. Calculated overpotentials as a function of H-coverage on oxidized Mo_2X monolayers: (**a**) differential Gibbs free energy for H atoms adsorbed on HC sites, (**b**) average Gibbs free energy for H atoms adsorbed on HC sites, (**c**) differential Gibbs free energy for H atoms adsorbed on TX sites, (**b**) average Gibbs free energy for H atoms adsorbed on TX sites.

and M_2XO_2-mH-Ad are larger than those of M_2X (Supporting data, Table T1). Because of possible phase transition during hydrogen evolution reaction, both adsorption sites (HC and TX) are considered when calculating Gibbs free energies.

Similarly, a supercell with $2 \times 2 \times 1$ unit cells is constructed based on the unit of M_2XO_2-mH-Ad (m = 1 and 2, Ad = HC and TX). By removing H atom one by one from a H-covered surface, the H-coverage dependent HER activity can be evaluated. The DFT-calculated Gibbs free energies show that Mo_2X monolayers with oxidization at HC sizes are better than those at TX sites in HER activities (Fig. 6). Mo_2XO_2-1H-HC (X = C and N) shows the best HER performance at n = 2 ($d\text{-}\Delta G_H = -0.03 \sim 0.03$ eV), and the HER activities of Mo_2XO_2-2H-HC are better

if $1 < n < 2$ where the d-ΔG_H cross the reference line (0 eV) in individual processes (Fig. 6a). Importantly, the a-ΔG_H of Mo_2XO_2-1H-HC (X = C and N) at full H-coverage (n = 4) are near-zero (0.01~0.04 eV, Fig. 6b), indicating the collective processes can take place. It is expected that the collective HER process on Mo_2XO_2-1H-HC is dominant at high H-density, and the individual processes may take over the role when H-density is low. Similarly, the collective processes of Mo_2XO_2-2H-HC can take place within the H-coverage from 2 to 3 (Fig. 6b). For Mo_2X monolayers with oxidization at TX, only Mo_2CO_2-2H-TX shows high HER activity at low H-coverage (n = 1, $\Delta G_H = 0.02$ eV) (Fig. 6c,d). Although the oxidization results in the improvement of the HER performances of W_2CO_2 monolayers with O atoms at HC sites at low H-coverage, but their HER activities at high H-coverage are greatly reduced (Supporting data, S-2a,b). W_2CO_2 monolayers with O atoms at TX sites shows poor HER performances (S-2c,d). Our calculations also show that W_2NO_2 monolayers with partial H-coverage ($0 < n < 4$) are unstable and their Gibbs free energies are not calculated.

Discussion

By systematically analysing the HER activities of pure and functionalized M_2X monolayers with various H-adsorption configurations, it is found that the HER activity of MXene strongly depends on its composition, hydrogen adsorption configuration, and surface functionalization. Generally, the less stable adsorption, the better HER activity. It is found that pure and hydrogen-functionalized W_2C monolayers shows the best HER performance at high H-coverage among all of considered systems, and is comparable to Pt because of near-zero overpotential. The overpotentials of pure W_2C monolayer at full H-coverage in individual process decreases from 0.15 eV to 0.05 eV, then to 0.02 eV as the H-adsorption site changing from HC → TX → TM (Fig. 3a,c,e). The hydrogen functionalization can efficiently improve the HER activity of W_2C monolayer. Almost zero Gibbs free energies at high H-coverage in individual processes can be achieved on W_2CH regardless of H-adsorption sites (Fig. 4a,c,e). Importantly, both differential and average Gibbs free energies of W_2C-TM and W_2CH-TM are within a range of −0.2 to 0.1 eV in the whole H-coverage (n = 1~4) (Figs 3e,f and 4e,f), indicating its excellent performance in hydrogen evolution reaction. Their HER activities are much better than MX_2 monolayers and nanoribbons when considering the H-coverage density and oeverpotentials, where 2D MX_2 only showed high activities at certain H-density[23,26,29–35,54,55] (Supporting data, Table S-2). A recent work on V_2CO_2 was noticed during revision, which showed that pure monolayer is worse on HER, while metal-decoration on its surface could improve its HER performance at certain H-coverage[56]. My calculations predict that pure W_2C, W_2CH and Mo_2XO_2 (X = C and N) monolayers show better HER performances with near-zero Gibbs free energies in wide range of H-coverages than Ni-V_2CO_2 (Table S-2). Although H atoms prefer to occupy HC or TX sites on W_2C monolayer (Fig. 2), the H adsorption on TM is also exothermic and the energy is only higher than those on HC and TX by 0.20~0.35 eV/unit. In experiments, H atoms may first approach to TM sites because metal layers are outmost, and then HER reactions occurs accordingly. Interestingly, the oxidized W_2C monolayers show better HER activities with near-zero Gibbs free energy at low H-coverage, but worse at high H-coverage (S-2a,b). It is, therefore, suggested that acid solution is required in HER reactions to avoid oxidization and keep the HER performance of W_2C monolayer. Different from oxidized W_2C monolayers, the oxygen functionalized Mo_2X monolayers shows excellent HER catalytic activities at medium H-coverage (n = 2) in individual processes (Fig. 6a) and at high H-coverage in collective processes (Fig. 6b). Especially, the average Gibbs free energies of Mo_2XO_2-1H-HC at full H-coverage (n = 4) in collective processes are 0.02~0.04 eV (Fig. 6b). Compared with pure and H-functionalized Mo_2X monolayers (Figs 3 and 4), it is found that oxidization can dramatically improve their HER activities at full H-coverage in collective processes (Fig. 6b), but their HER performances at low H-coverage are greatly reduced.

Conclusions

I carries out first-principles calculations to investigate the catalytic activities of MXenes for applications into HER. It is found that pure and hydrogenated W_2C monolayers are better than other MXenes without oxygen functionalization and show the best HER performances at high H-density in HER reactions because of near-zero overpotential. In particular, excellent HER performance in the whole H-coverage from zero to full can be achieved on W_2C monolayers with H atoms adsorbed on the top of W atoms, which can be realized by controlling experimental conditions. However, the optimal HER activity of W_2C monolayer is degraded if it is oxidized or functionalized by oxygen atoms, especially at high H-coverage. It is further shown that the oxidization can dramatically improve the HER activities of Mo_2X monolayers. The oxidized Mo_2X monolayers exhibit best HER performances in individual processes at medium H-coverage and in collective processes at high H-coverage due to near-zero Gibbs free energies. For practical applications in experiments, I suggest that oxidization should be avoided to keep the advanced HER activity of W_2C monolayer used as electrocatalyst, while Mo_2X monolayers may need to be functionalized by oxygen to enhance their activities. The MXenes with activity comparable to novel metals may be obtained by tuning compositions and functionalizing, and find applications into HER reactions.

Methods

The first-principles calculations are carried out to investigate the hydrogen evolution reaction of MXenes. The calculations are based on the density functional theory (DFT)[57] and the Perdew-Burke-Eznerhof generalized gradient approximation (PBE-GGA)[58]. The projector augmented wave (PAW) scheme[59,60] as incorporated in the Vienna ab initio simulation package (VASP)[61] is used in the study. The Monkhorst and Pack scheme of k-point sampling is used for integration over the first Brillouin zone[62]. A $15 \times 15 \times 1$ grid for k-point sampling for geometry optimization of unit cells, and an energy cut-off of 500 eV are consistently used in our calculations. A sufficiently large supercell is used so that the monolayers in neighbouring cells in the vertical direction are separated

by a vacuum region of at least 20 Å. Dipole correction is not included. Good convergence is obtained with these parameters and the total energy was converged to 2.0×10^{-5} eV/atom. The error bar (or uncertainty) of the DFT calculation is less than 5 meV.

References

1. Mallouk, T. E. Water electrolysis: Divide and conquer. *Nat. Chem.* **5,** 362–363 (2013).
2. Dincer, I. & Acar, C. Review and evaluation of hydrogen production methods for better sustainability. *Int. J. Hydrogen Energy* **40,** 11094–11111 (2015).
3. Wang, J., Zhang, Y., Capuano, C. B. & Ayers, K. E. Ultralow charge-transfer resistance with ultralow Pt loading for hydrogen evolution and oxidation using Ru@Pt core-shell nanocatalysts. *Sci. Rep.* **5,** 12220 (2015).
4. Liu, X., Zheng, H. F., Sun, Z. J., Han, A. & Du, P. W. Earth-abundant copper-based bifunctional electrocatalyst for both catalytic Hydrogen Production and water oxidation. *ACS Catal.* **5,** 1530–1538 (2015).
5. Strmcnik, D. *et al.* The role of non-covalent interactions in electrocatalytic fuel-cell reactions on platinum. *Nat. Chem.* **1,** 466–472 (2009).
6. Patel, P. P. *et al.* Nanostructured robust cobalt metal alloy based anode electro-catalysts exhibiting remarkably high performance and durability for proton exchange membrane fuel cells. *J. Mate. Chem. A* **3,** 14015–14032 (2015).
7. Koh, S. & Strasser, P. Electrocatalysis on bimetallic surfaces: modifying catalytic reactivity for oxygen reduction by voltammetric surface dealloying. *J. Am. Chem. Soc.* **129,** 12624–12625 (2007).
8. Gressley, J., Jarmaillo, T. F., Bonde, J., Chorkendorff, I. & Nørskov, J. K. Computational high-throughput screening of electrocatalytic materials for hydrogen evolution. *Nat. Mater.* **5,** 909–913 (2006).
9. Norskov, J. K., Bligaard, T., Rossmeisl, J. & Christensen, C. H. Towards the computational design of solid catalysts. *Nat. Chem.* **1,** 37–46 (2009).
10. Karlberg, G. S. *et al.* Cyclic voltammograms for H on Pt(111) and Pt(100) from first principles. *Phys. Rev. Lett.* **99,** 126101 (2007).
11. Pan, H., Feng, Y. P. & Lin, J. Y. Enhancement of hydrogen evolution on tungsten doped platinum. *J. Comput. Theor. Nanosci.* **7,** 547–551 (2010).
12. Xia, B. Y. *et al.* One-pot synthesis of Pt-Co alloy nanowire assemblies with tunable composition and enhanced electrocatalytic properties. *Angew. Chem. Int. Ed.* **54,** 3797–3801 (2015).
13. Lim, C. S., Tan, S. M., Sofer, Z. & Pumera, M. Impact electrochemistry of layered transition metal dichalcogenides. *ACS Nano* **9,** 8474–8583 (2015).
14. Yu, L., Xia, B. Y., Wang, X. & Lou, X. W. General formation of M-MoS_3 (M = Co, Ni) hollow structures with enhanced electrocatalytic activity for hydrogen evolution. *Adv. Mater.* **28,** 92–97 (2016).
15. Falkowski, J. M. & Surendranath, Y. Metal chalcogenide nanofilms: platforms for mechanistic studies of electrolysis. *ACS Catal.* **5,** 3411–3416 (2015).
16. Wu, H. B., Xia, B. Y., Yu, L., Yu, X. Y. & Lou, X. W. Porous molybdenum carbide nano-octahedrons synthesized via confined carburization in metal-organic frameworks for efficient hydrogen production. *Nat. Commun.* **6,** 6512 (2015).
17. Chen, W. F., Muckerman, J. T. & Fujita, E. Recent developments in transition metal carbides and nitrides as hydrogen evolution electrocatalysts. *Chem. Commun.* **49,** 8896–8909 (2013).
18. Ma, F. X., Wu, H. B., Xia, B. Y., Xu, C. Y. & Lou, X. W. Hierarchical β-Mo_2C nanotubes organized by ultrathin nanosheets as a highly efficient electrocatalyst for hydrogen production. *Angew. Chem. Int. Ed.* **54,** 15395–15399 (2015).
19. Xu, M. *et al.* Porous CoP concave polyhedron electrocatalysts synthesized from metal-organic frameworks with enhanced electrochemical properties for hydrogen evolution. *J. Mater. Chem. A* **3,** 21471–21477 (2015).
20. Yu, X. Y., Yu, Y., Wu, H. B. & Luo, X. W. Formation of nickel sulfide nanoframes from MOFs with enhanced eseudocapacitive and electrocatalytic properties. *Angew. Chem. Int. Ed.* **54,** 5331–5335 (2015).
21. Jaramillo, T. F. *et al.* Identification of active edge sites for electrochemical H_2 evolution from MoS_2 nanocatalysts. *Science* **317,** 100–102 (2007).
22. Karunadasa, H. I. *et al.* Molecular MoS_2 edge site mimic for catalytic hydrogen generation. *Science* **335,** 698–702 (2012).
23. Tsai, C., Chan, K., Nørskov, J. K. & Abild-Pedersen, F. Rational design of MoS_2 catalysts: Tuning the structure and activity via transition metal doping. *Catal. Sci. Technol.* **5,** 246–253 (2015).
24. Yu, X. Y., Hu, H., Wang, Y. W., Chen, H. Y. & Luo, X. W. Ultrathin MoS_2 nanosheets supported on N-doped carbon nanoboxes with enhanced Lithium storage and electrocatalytic properties. *Angew. Chem. Int. Ed.* **54,** 7395–7398 (2015).
25. Kibsgaard, J., Chen, Z., Reinecke, B. N. & Jaramillo, T. F. Engineering the surface structure of MoS2 to preferentially expose active edge sites for electrocatalysis. *Nat. Mater.* **11,** 963–969 (2012).
26. Voiry, D. *et al.* Covalent functionalization of monolayered transition metal dichalcogenides by phase engineering. *Nat. Chem.* **7,** 45–49 (2014).
27. Zhang, L., Wu, H. B., Yan, Y., Wang, X. & Luo, X. W. Hierarchical MoS_2 microboxes constructed by nanosheets with enhanced electrochemical properties for Lithium storage and water splitting. *Energy Environ. Sci.* **7,** 3302–3306 (2014).
28. Ambrosi, A., Sofer, Z. & Pumera, M. 2H → 1T phase transition and hydrogen evolution activity of MoS_2, $MoSe_2$, WS_2 and WSe_2 strongly depends on the MX_2 composition. *Chem. Commun.* **51,** 8450–8453 (2015).
29. Tsai, C., Chan, K., Abild-Pedersen, F. & Nørskov, J. K. Active edge sites in $MoSe_2$ and WSe_2 catalysts for the hydrogen evolution reaction: a density functional study. *Phys. Chem. Chem. Phys.* **16,** 13156–13164 (2014).
30. Qu, Y., Pan, H., Kwok, C. T. & Wang, Z. A first-principles study on the hydrogen evolution reaction of VS_2 nanoribbons. *Phys. Chem. Chem. Phys.* **17,** 24820–24825 (2015).
31. Voiry, D. *et al.* Enhanced catalytic activity in strained chemically exfoliated WS_2 nanosheets for hydrogen evolution. *Nat. Mater.* **13,** 850–855 (2013).
32. Tsai, C., Abild-Pedersen, F. & Nørskov, J. K. Tuning the MoS_2 edge-site activity for hydrogen evolution via support interactions. *Nano Lett.* **14,** 1381–1387 (2014).
33. Pan, H. Metal dichalcogenides monolayers: novel catalysts for electrochemical hydrogen production. *Sci. Rep.* **4,** 5438 (2014).
34. Wu, Z. Z. *et al.* MoS_2 nanosheets: a designed structure with high active site density for the hydrogen evolution reaction. *ACS Catal.* **3,** 2101–2107 (2013).
35. Chen, T. Y. *et al.* Comparative study on MoS_2 and WS_2 for electrocatalytic water splitting. *Int. J. Hydro. Energy* **38,** 12302–12309 (2013).
36. Naguib, M., Mochalin, V. N., Barsoum, M. W. & Gogotsi, Y. MXenes: a new family of two-dimensional materials. *Adv. Mater.* **26,** 992–1005 (2014).
37. Wang, X. F. *et al.* Atomic-scale recognition of surface structure and intercalation mechanism of Ti_3C_2X. *J. Am. Chem. Soc.* **137,** 2715–2721 (2015).
38. Ji, X. *et al.* Different charge-storage mechanisms in disulfide vanadium and vanadium carbide monolayer. *J. Mater. Chem. A.* **3,** 9909–9914 (2015).
39. Ling, Z. *et al.* Flexible and conductive MXene films and nanocomposites with high capacitance. *J. Am. Chem. Soc.* **111,** 16676–16681 (2014).

40. Eames, C. & Islam, M. S. Ion intercalation into two-dimensional transition-metal carbides: global screening for new high-capacity battery materials. *J. Am. Chem. Soc.* **136,** 16270–16276 (2014).
41. Hu, J. P., Xu, B., Ouyang, C. Y., Yang, S. Y. A. & Yao, Y. G. Investigations on V_2C and V_2CX_2 (X = F, OH) mono layer as a promising anode material for Li ion batteries from first-principles calculations. *J. Phys. Chem. C* **118,** 24274–24281 (2014).
42. Pan, H. Electronic properties and lithium storage capacities of two-dimensional transition-metal nitrides monolayers. *J. Mater. Chem. A.* **3,** 21486–21493 (2015).
43. Xie, Y. *et al.* Role of surface structure on Li-ion energy storage capacity of two-dimensional transition-metal carbides. *J. Am. Chem. Soc.* **136,** 6385–6394 (2014).
44. Jing, Y., Zhou, Z., Cabrera, C. R. & Chen, Z. F. Graphene, inorganic graphene analogs and their composites for lithium ion batteries. *J. Mater. Chem. A* **2,** 12104–12122 (2014).
45. Lukatskaya, M. R. *et al.* Cation intercalation and high volumetric capacitance of two-dimensional titanium carbide. *Science* **341,** 1502–1505 (2013).
46. Tang, Q., Zhou, Z. & Shen, P. W. Are MXenes promising anode materials for Li ion batteries? computational studies on electronic properties and Li storage capability of Ti_3C_2 and $Ti_3C_2X_2$ (X = F, OH) monolayer. *J. Am. Chem. Soc.* **134,** 16909–16916 (2012).
47. Mashtalir, O. *et al.* Intercalation and delamination of layered carbides and carbonitrides. *Nat. Commun.* **4,** 1716 (2013).
48. Lei, J. C., Zhang, X. & Zhou, Z. Recent advances in MXene: Preparation, properties, and applications. *Front. Phys.* **10,** 276–286 (2015).
49. Tang, Q. & Zhou, Z. Graphene-analogous low-dimensional materials. *Prog. Mater. Sci. 2013* **58,** 1244–1315 (2013).
50. Zhang, X., Ma, Z. N., Zhao, X. D., Tang, Q. & Zhou, Z. Computational studies on structural and electronic properties of functionalized MXene monolayers and nanotubes. *J. Mater. Chem. A* **3,** 4960–4966 (2015).
51. Xie, Y. & Kent, P. R. C. Hybrid density functional study of structural and electronic properties of functionalized $Ti_{n+1}X_n$ (X = C, N) monolayers. *Phys. Rev. B* **87,** 235441 (2013).
52. Xu, C. *et al.* Large-area high-quality 2D ultrathin Mo_2C superconducting crystals. *Nat. Mater.* **14,** 1135–1141 (2015).
53. Nørskov, J. K. *et al.* Trends in the exchange current for hydrogen evolution. *J. Electrochem. Soc.* **152,** J23–J26 (2005).
54. Pan, H. Tension-enhanced hydrogen evolution reaction on vanadium disulfide monolayer. *Nanoscale Res. Lett.* **11,** 113 (2016).
55. Fan, X. L., Wang, S. Y., An, Y. R. & Lau, W. M. Catalytic activity of MS_2 monolayer for electrochemical hydrogen evolution. *J. Phys. Chem. C* **120,** 1623–1632 (2016).
56. Ling, C. Y., Shi, L., Ouyang, Y. X., Chen, Q. & Wang, J. L. Transition metal-promoted V_2CO_2 (MXenes): A new and highly active catalyst for hydrogen evolution reaction. *Adv. Sci.* 1600180 (2016).
57. Hohenberg, P. & Kohn, W. Inhomogeneous electron gas. *Phys. Rev.* **136,** B864–B871 (1964).
58. Blöchl, P. E. Projector augmented-wave method. *Phys. Rev. B* **50,** 17953–17979 (1994).
59. Perdew, J. P., Burke, K. & Ernzerhof, M. Generalized gradient approximation made simple. *Phys. Rev. Lett.* **77,** 3865–3868 (1996).
60. Kresse, G. & Joubert, D. From ultrasoft pseudopotentials to the projector augmented-wave method. *Phys. Rev. B* **59,** 1758–1775 (1999).
61. Kresse, G. & Furthmuller, J. Efficient iterative schemes for ab initio total-energy calculations using a plane-wave basis set. *Phys. Rev. B* **54,** 11169–11186 (1996).
62. Monkhorst, H. J. & Pack, J. Special points for brillouin-zone integrations. *Phys. Rev. B* **13,** 5188–5192 (1976).

Acknowledgements

Hui Pan thanks the support of the Science and Technology Development Fund from Macau SAR (FDCT-068/2014/A2, FDCT-132/2014/A3, and FDCT-110/2014/SB) and Multi-Year Research Grant (MYRG2014-00159-FST and MYRG2015-00017-FST) from Research & Development Office at University of Macau. The DFT calculations were performed at High Performance Computing Cluster (HPCC) of Information and Communication Technology Office (ICTO) at University of Macau.

Author Contributions

H.P. conceived the idea, performed the calculations, and wrote the paper.

Additional Information

Supplementary information accompanies this paper at http://www.nature.com/srep

Competing financial interests: The authors declare no competing financial interests.

How to cite this article: Pan, H. Ultra-high electrochemical catalytic activity of MXenes. *Sci. Rep.* **6**, 32531; doi: 10.1038/srep32531 (2016).